Delft University of Technology

High-Strength Amorphous Silicon Carbide for Nanomechanics

Xu, Minxing; Shin, Dongil; Sberna, Paolo M.; van der Kolk, Roald; Cupertino, Andrea; Bessa, Miguel A.; Norte, Richard A.

DOI
10.1002/adma.202306513

Publication date
2023

Document Version
Final published version

Published in
Advanced Materials

Citation (APA)
Xu, M., Shin, D., Sberna, P. M., van der Kolk, R., Cupertino, A., Bessa, M. A., & Norte, R. A. (2023). High-Strength Amorphous Silicon Carbide for Nanomechanics. *Advanced Materials*, *36*(5), Article 2306513. https://doi.org/10.1002/adma.202306513

Important note
To cite this publication, please use the final published version (if applicable).
Please check the document version above.

Copyright
Other than for strictly personal use, it is not permitted to download, forward or distribute the text or part of it, without the consent of the author(s) and/or copyright holder(s), unless the work is under an open content license such as Creative Commons.

Takedown policy
Please contact us and provide details if you believe this document breaches copyrights.
We will remove access to the work immediately and investigate your claim.

This work is downloaded from Delft University of Technology.
For technical reasons the number of authors shown on this cover page is limited to a maximum of 10.

Check for updates

ADVANCED MATERIALS
www.advmat.de

High-Strength Amorphous Silicon Carbide for Nanomechanics

Minxing Xu, Dongil Shin, Paolo M. Sberna, Roald van der Kolk, Andrea Cupertino, Miguel A. Bessa, and Richard A. Norte**

For decades, mechanical resonators with high sensitivity have been realized using thin-film materials under high tensile loads. Although there are remarkable strides in achieving low-dissipation mechanical sensors by utilizing high tensile stress, the performance of even the best strategy is limited by the tensile fracture strength of the resonator materials. In this study, a wafer-scale amorphous thin film is uncovered, which has the highest ultimate tensile strength ever measured for a nanostructured amorphous material. This silicon carbide (SiC) material exhibits an ultimate tensile strength of over 10 GPa, reaching the regime reserved for strong crystalline materials and approaching levels experimentally shown in graphene nanoribbons. Amorphous SiC strings with high aspect ratios are fabricated, with mechanical modes exceeding quality factors 10^8 at room temperature, the highest value achieves among SiC resonators. These performances are demonstrated faithfully after characterizing the mechanical properties of the thin film using the resonance behaviors of free-standing resonators. This robust thin-film material has significant potential for applications in nanomechanical sensors, solar cells, biological applications, space exploration, and other areas requiring strength and stability in dynamic environments. The findings of this study open up new possibilities for the use of amorphous thin-film materials in high-performance applications.

1. Introduction

Advances in nanotechnology have revolutionized various fields, with the development of tensile-loaded, thin-film mechanical devices playing a pivotal role in state-of-the-art force, acceleration, and displacement sensing.[1–7] Two approaches are used to boost the sensitivity of nanomechanical resonators under tensile loads. One approach fabricates the resonators using different materials in pursuit of films with inherent high-stress and low mechanical loss tangents (i.e high mechanical quality factors). In room temperature environments, high-tensile amorphous silicon nitride (a-Si_3N_4) nanomechanical resonators have marked some of the best performing devices in ultrasensitive mechanical detectors.[8–13] Crystalline thin film materials (e.g. crystalline silicon (c-Si),[14] crystalline silicon carbide (c-SiC)[15,16]) and graphene are expected to have higher theoretical limits, but their projected performance relies on having perfect crystal structures with no defects (including edge defects). Additionally, it is difficult to attain crystalline films[14,15] that can be easily deposited, have good film isotropy,[17] and few lattice imperfections.[14,15]

The other approach to boost sensor performance involves innovative resonator designs that concentrate stress in key areas. These designs are constrained by the thin film materials' tensile fracture limits or ultimate tensile strength (UTS). Nanostructuring reduces the UTS due to introduced

M. Xu, D. Shin, A. Cupertino, R. A. Norte
Department of Precision and Microsystems Engineering
Delft University of Technology
Delft, CD 2628, The Netherlands
E-mail: r.a.norte@tudelft.nl

M. Xu, R. A. Norte
Department of Quantum Nanoscience
Delft University of Technology, Kavli Institute of Nanoscience
Delft, CD 2628, The Netherlands

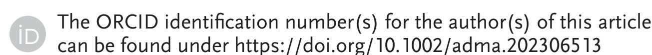
The ORCID identification number(s) for the author(s) of this article can be found under https://doi.org/10.1002/adma.202306513

© 2023 The Authors. Advanced Materials published by Wiley-VCH GmbH. This is an open access article under the terms of the Creative Commons Attribution License, which permits use, distribution and reproduction in any medium, provided the original work is properly cited.

DOI: 10.1002/adma.202306513

D. Shin
Department of Materials Science and Engineering
Delft University of Technology
Delft, CD 2628, The Netherlands

P. M. Sberna
Faculty of Electrical Engineering
Mathematics and Computer Science
Delft University of Technology, Else Kooi Laboratory
Delft, CD 2628, The Netherlands

R. van der Kolk
Department of Quantum Nanoscience
Delft University of Technology, Kavli Nanolab
Delft, CD 2628, The Netherlands

M. A. Bessa
Brown University
School of Engineering
Providence, RI 02912, USA
E-mail: miguel_bessa@brown.edu

15214095, 0, Downloaded from https://onlinelibrary.wiley.com/doi/10.1002/adma.202306513 by Technical University Delft, Wiley Online Library on [12/12/2023]. See the Terms and Conditions (https://onlinelibrary.wiley.com/terms-and-conditions) on Wiley Online Library for rules of use; OA articles are governed by the applicable Creative Commons License

Table 1. LPCVD a-SiC deposition parameters and the corresponding mechanical properties. From left to right columns, recipe name, gas flow ratio (GFR), deposition pressure P, thickness t, deposition stress σ, density ρ, Young's modulus E, Poisson ratio ν, intrinsic quality factor Q_0 (per 100 nm), and ultimate tensile strength (UTS), are shown. All a-SiC recipes have a deposition time 3 h 20 min, except a-SiCR2FS (3 h 47 min). Note that the mechanical properties of a-SiCR2FS are characterized with alternative methods presented in Section S(A5) (Supporting Information).

Recipe	GFR	P [mTorr]	Substrate	t [nm]	σ [MPa]	ρ [kg m^{-3}]	E [GPa]	ν	Q_0	UTS [GPa]
a-SiCR2	2	600	Silicon	71	760	2830	223	0.203	5175	12.04 (±0.72)
a-SiCR2FS	2	600	Fused Silica	82	1404	2555	187	0.222	4416	-
a-SiC170	2	170	Silicon	86	636	2966	220	0.218	4485	10.27 (±0.62)
a-SiCR3	3	600	Silicon	81	960	2962	210	0.199	4692	11.12 (±0.45)
a-SiCR4	4	600	Silicon	137	670	3087	200	0.162	1035	<3.5

crystalline defects.[18,19] For example, the UTS of a-Si_3N_4 thin film has been shown to be 6.8 GPa.[20] To date, only crystalline and 2D materials have experimentally demonstrated UTS surpassing 10 GPa after being top-down nanofabricated.[21–24] Among 2D crystalline materials, graphene harbors one of the highest theoretical UTS,[23,25] but practically reaching the limit is also challenging due to lattice imperfections,[26] atomically irregular edges,[24] or sparser grain boundaries[27] resulting from nanostructuring processes, which lead to a reduced fracture limit when it is tensile-loaded. In this regard, amorphous thin films with high UTS offer more design freedom for free-standing nanostructures, due to their lack of both crystalline defects and sensitivity to notches.[28–31] Apart from allowing the enhancement of the Q factor of nanomechanical resonators, higher material UTS can enable the devices to perform better in diverse and harsh vibrational environments.

Amorphous SiC (a-SiC) thin film is gaining traction due to its remarkable mechanical strength and versatile properties.[32–34] It holds unique advantages over its crystalline counterparts, such as lower deposition temperature and adaptability to various substrates,[35,36] enabling deposition on large wafer scales. This material stands out in applications requiring protective coatings and in the development of MEMS sensors and integrated photonics, due to its resilience to mechanical wear[37] and chemical corrosion.[38] Its potential in high-yield production of diverse devices paves the way for advancements in sensing[6] and quantum technology.[39]

In this work, we demonstrate wafer-scale amorphous films that harbor an ultimate tensile strength over 10 GPa after nanostructuring, a regime that is conventionally reserved for ultra-strong crystalline and 2D materials. Using delicate nanofabrication techniques, we produce several different nanomechanical resonators that can accurately determine the mechanical properties of SiC thin films such as density, Young's modulus, Poisson ratio, and ultimate tensile strength. Notably, our highest measured tensile strength (>10 GPa) is comparable to the values shown for c-SiC[21] and approaching the experimental values obtained for double-clamped graphene nanoribbon.[24] We achieve mechanical quality factor up to 2×10^8 with a-SiC mechanical resonators, and measure loss-tangents on par with other materials used in high-precision sensors. Beyond sensing, these strong films open up new possibilities in high-performance nanotechnology, including thin solar cell technologies,[40] mechanical sensing,[41] biological technologies[42] and even lightsail space exploration.[43]

2. Fabrication of Amorphous SiC Resonators

In pursuit of thin film materials for nanomechanical resonators with low mechanical dissipation, high film quality and high tensile stress are desirable. The low-pressure chemical vapor deposition (LPCVD) technique is preferred for these requirements, since its low pressure and high temperature deposition environment ensures lower defect density and higher thermal stress. The non-stoichiometric LPCVD a-SiC films used in this paper are deposited with different gas flow ratios (GFR) between SiH_2Cl_2 and 5% C_2H_2 in H_2 (GFR = 2, 3, 4), various deposition pressures (170 and 600 mTorr), and on both silicon and fused silica substrates (**Table 1**). This variation of deposition parameters allow us to systematically characterize the mechanical properties of LPCVD a-SiC thin films. All a-SiC thin films were deposited for the same period of time (3 h 20 min) at a temperature of 760 °C in order to better determine the effect of various deposition environments while maintaining the films in the amorphous form.[44] With the fabrication process demonstrated in the Experimental Section, nanomechanical resonators made of a-SiC can be suspended over the substrates with high yield using dry etching processes due to their extremely high chemical selectivity.

Higher chemical stability and inertness of thin films is particularly useful for suspending nanostructures; usually a crucial and difficult step in fabricating free-standing structures. LPCVD a-SiC films can be deposited on various substrates, patterned, and then suspended as nanomechanical resonators by removing the substrate underneath (i.e. undercutting). A high selectivity between the thin film and the substrate allows for higher yield and accuracy in fabricating suspended nanostructures. Similar to their crystalline counterpart, LPCVD a-SiC thin films have been reported to have very high chemical inertness to various wet etchants.[35] Likewise, we found that a-SiC also has high chemical inertness to the widely used dry etchants, such as SF_6 isotropic plasma etching for silicon substrate, and vapor hydrofluoric acid etching for silicon oxide substrate, as illustrated in **Figure 1**a. The excellent chemical stability implies high selectivity between a-SiC and various commonly used substrates during

© 2023 The Authors. Advanced Materials published by Wiley-VCH GmbH

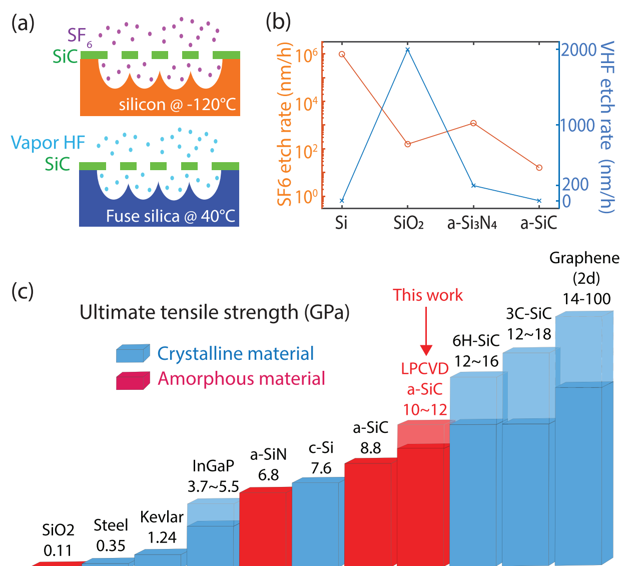

Figure 1. a) Schematic of dry undercut processes with cryogenic SF_6 plasma isotropic etching (top) and vapor hydrofluoric acid etching (bottom), to suspend a-SiC nanomechanical resonators (green) on silicon (orange) and fused silica (blue) substrates, respectively. b) Etch rates of cryogenic SF_6 plasma isotropic etching (log scale) and vapor hydrofluoric acid etching (linear scale), on four commonly used Si-based materials: Si, SiO_2, a-Si_3N_4, and a-SiC. c) Ultimate tensile strength comparison between LPCVD a-SiC, crystalline (blue), and amorphous (red) materials. References: SiO_2,[45] steel,[46] Kevlar,[47] InGaP,[17] a-Si_3N_4,[9,20] c-Si,[41,48] a-SiC,[49] 6H-SiC (crystalline),[21] 3C-SiC (crystalline),[21] and graphene.[22,24] The solid and transparent colors of bars represent the lower and upper limits of the materials' ultimate tensile strengths, respectively.

undercutting, as shown in Figure 1b. Dry etchants are preferred for suspending high-aspect-ratio nanomechanical structures, since they help to avoid stiction during liquid etchant evaporation and thus improve the yield rate of working devices. To demonstrate the range of devices possible with higher chemical inertness, we fabricated nanomechanical resonators with continuous films down to 5nm, as shown in SEM pictures in Section SF (Supporting Information). In Section SH (Supporting Information) ,we show the measured chemical composition of these films, and demonstrate the chemical integrity of the 5 nm SiC after etching.

The undercut method based on dry etchants introduces little perturbation to the suspended nanostructure, making it possible to perform delicate, on-chip tensile testing. The precision of the undercut method is pivotal for the reliability of material strength testing as it mitigates the risks associated with introducing fractures and defects during the loading/gluing of a material into a tensile testing setup, which could compromise the integrity of maximum tensile strength measurements. This chemical inertness of a-SiC serves a functional role in the fabrication process, allowing for a high degree of compatibility with various undercuts and ensuring the integrity of the nanostructures during the suspension process. The inertness contributes to the overall reliability and accuracy of the UTS measurements by inducing minimal forces during both fabrication and testing. In Section 4, we fabricate suspended nanostructures with different maximum tensile stresses to accurately determine the ultimate tensile strength (UTS) of a-SiC films. As a result, we demonstrate that a-SiC films have UTS up to 10–12 GPa, which are the highest among amorphous materials after patterning and are approaching the UTS of strong materials like c-SiC[21] and graphene nanoribbons,[24] both of which are known for their high UTS. The comparison of UTS between LPCVD a-SiC and other materials commonly used for nanomechanics is shown in Figure 1c.

3. Mechanical Property Characterization With Resonance Method

In order to design desired nanomechanical resonators with a specific thin film material, it is necessary to accurately characterize the material's mechanical parameters, such as film stress, Young's modulus, Poisson ratio and density. Various methods are developed to measure these parameters, including static methods, like nano-indentation[50,51] and dynamic methods like resonance response.[52–55] Many studies aiming to design high-performance nanomechanical resonators have relied on mechanical parameter values obtained from the literature without considering potential variations of thin film properties due to different deposition environments, such as commonly used materials like a-Si_3N_4,[10,12] c-Si,[14] and c-SiC.[15,16] While these adaptations are usually reasonable and align well with experimental results, characterizing the exact parameters of the materials used would be beneficial when exploring the optimal performance of nanomechanical resonators.[52,56] In this section, we present a simple and universal method to systematically characterize the important mechanical parameters of LPCVD a-SiC thin films.

The characterization flow of the method begins with measuring the thickness of the a-SiC thin film (t) after LPCVD deposition using a spectroscopic ellipsometer, which is an optical technique to confirm the thin film thickness and investigate its dielectric properties simultaneously. We then identify the film stress (σ) using the wafer bending method. After dicing the wafer into small chips, we pattern the a-SiC thin film and suspend it in the form of membranes, cantilevers, and strings with different lengths (L). The suspended nanomechanical resonators are measured with a laser Doppler vibrometer (LDV) in the vacuum environment down to 10^{-7} mbar. The measured resonant frequencies of the fundamental modes of the membranes (f_{mem}), cantilevers (f_{can}), and strings (f_{str}) can be fitted with their corresponding analytical expressions, which reveal the Young's modulus (E), Poisson ratio (ν), and density (ρ) of the a-SiC thin film, respectively. During the fitting process, finite element method (FEM) simulation is used to describe the patterned resonators more precisely by taking into account the holes on the membranes and the overhangs from under-cutting adjacent to the cantilevers and strings. More detailed information about the measurements, analytical fitting, and simulations are shown in Sections SA and SB (Supporting Information)..

Using the above measurements, we can characterize the important mechanical parameters of LPCVD a-SiC thin films, then design and fabricate nanomechanical resonators with desired performance. Note that this straightforward and non-contact method can be universally applied to characterize the mechanical properties of other tensile thin film materials that can be fabricated into resonators with various geometries, for example

© 2023 The Authors. Advanced Materials published by Wiley-VCH GmbH

15214095, 0, Downloaded from https://onlinelibrary.wiley.com/doi/10.1002/adma.202306513 by Technical University Delft, Wiley Online Library on [12/12/2023]. See the Terms and Conditions (https://onlinelibrary.wiley.com/terms-and-conditions) on Wiley Online Library for rules of use; OA articles are governed by the applicable Creative Commons License

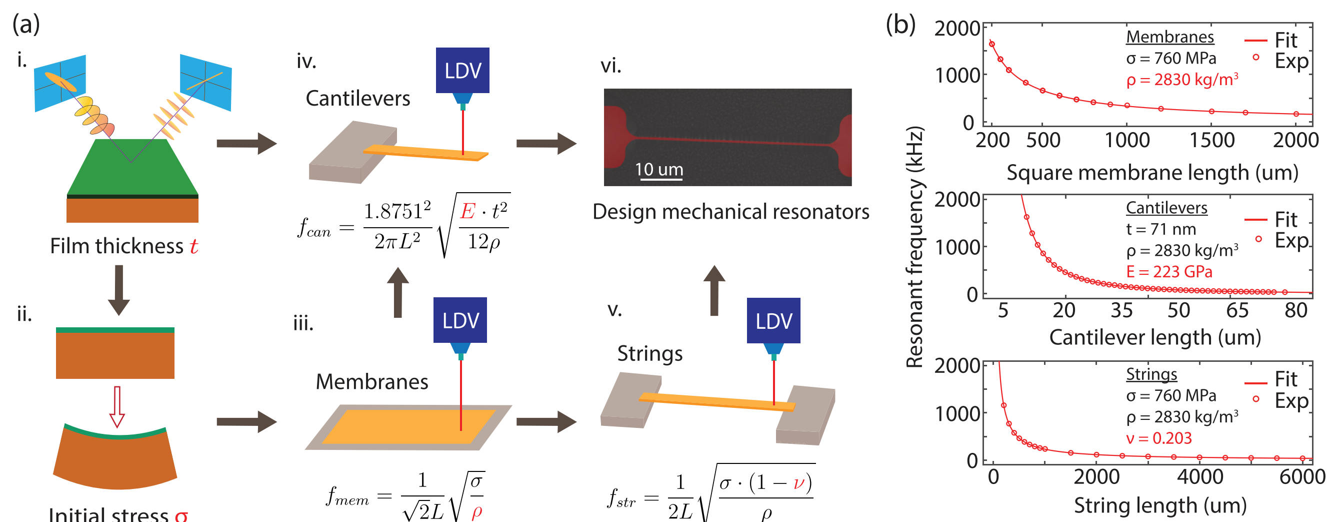

Figure 2. a) Schematic of systematically characterizing mechanical properties of a tensile stress thin film material. a-i) Measuring film thickness with ellipsometry. a-ii) Measuring the film stress via wafer bending technique after film deposition. a-iii) Extracting material density. a-iv) Young's modulus. a-v) Poisson ratio of a-SiC thin films by fitting resonant frequencies of square membranes/cantilevers/strings of different sizes, respectively. a-vi): Designing a-SiC nanomechanical resonators with desired performance. b) Characterizing the mechanical properties of LPCVD a-SiC thin film (a-SiCR2) by numerically fitting the measured resonant frequencies of suspended resonators with different geometries and dimensions, including squared membranes (top), cantilevers (middle), strings (bottom). The resonant frequencies of the resonators mentioned above are measured with a laser Doppler vibrometer (LDV, Polytec PSV-4).

cantilevers, strings, and membranes. This allows for quality control of thin films deposited in different batches or under varied deposition environments. As a result, nanomechanical resonators manufactured for various applications can be characterized in an efficient and economical manner, resulting in higher reliability for both industrial and academic applications. With all the relevant mechanical parameters accurately measured, we can fabricate a series of suspended devices specifically designed for characterizing the ultimate tensile strengths of a-SiC thin films in the following section.

4. Ultimate Tensile Strength of Amorphous SiC

Ultimate tensile strength (UTS), or sometimes coinciding with yield strength for brittle materials such as a-SiC,[49] describes the maximum tensile stress a material can endure before breaking while being stretched. High UTS has been shown for nanowires fabricated with various materials, whose small cross-section areas minimize the appearance of defects,[57,58] and for nanomechanical membranes without nanopatterning to avoid the presence of rough sidewalls.[59] However, both scenarios above do not allow for further shape modification, reducing interest in their potential for various applications. While the crystalline form of materials usually tend to be mechanically stronger than their amorphous forms due to long-range order, examples such as glassy metal[60] and synthesized AM-III carbon[61] demonstrate extraordinary mechanical properties comparable to their crystalline counterparts in terms of fracture toughness and yield strength, or hardness and compressive strength, respectively. This correspondence remains between c-SiC and a-SiC. While c-SiC has shown a UTS as high as 12–18 GPa via micro-pillars,[21] a-SiC nanowires have been measured to have a UTS up to 8.8 GPa via a tensile test with its two ends fixed by silver epoxy,[49] which is higher than the ones shown for LPCVD a-Si_3N_4 (6.8 GPa[20]) and Si (7.6 GPa[41]).

With the aim of characterizing the design space of nanomechanical resonators using LPCVD a-SiC thin film, we characterized its UTS by geometrically tapering the suspended a-SiC thin film in order to concentrate the tensile stress up to the fracture point. Unlike other tensile test methods,[62] the presented method allows to determine the UTS of the tensile nanostructured film accurately, while avoiding the ambiguity caused by external loads, glues, and limitations of nanofabrication; for example, limited accuracy of nanopatterning and stiction during wet undercut. With the mechanical parameters characterized in Section 3, a-SiC hourglass-shaped devices consisting of a short and narrow tether surrounded by long and wide pads on both sides that are designed and suspended to measure the UTS of LPCVD a-SiC thin films. The devices have a total length of 1500 μm, with pads on both sides that have a width of 15 μm, and the middle tethers that have varying lengths and a width of 500 nm, as shown in **Figures 2** and 3a. After being suspended with dry etchants, the tensile stress on the hourglass-shaped device will redistribute and result in an increase of stress on the middle tether due to the pulling of the pads caused by residual stresses arising from the fabrication. The re-distributed stress profile in Figure 3a is obtained via the finite element method (FEM). The devices are designed to have varying tether lengths from short to long, which are then arranged adjacently as shown in Figure 3b.

To establish a force equilibrium between the tether and the pads on each device, the ratio between the tensile stresses on the tether and the pads is inversely proportional to the ratio between their widths. Combined with a small proportion of the lengths between the two, which enhances the strain (percentage of elongation) on the tether, the tensile stress on the tether in our hourglass-shaped devices can be significantly amplified

© 2023 The Authors. Advanced Materials published by Wiley-VCH GmbH

15214095, 0, Downloaded from https://onlinelibrary.wiley.com/doi/10.1002/adma.202306513 by Technical University Delft, Wiley Online Library on [12/12/2023]. See the Terms and Conditions (https://onlinelibrary.wiley.com/terms-and-conditions) on Wiley Online Library for rules of use; OA articles are governed by the applicable Creative Commons License

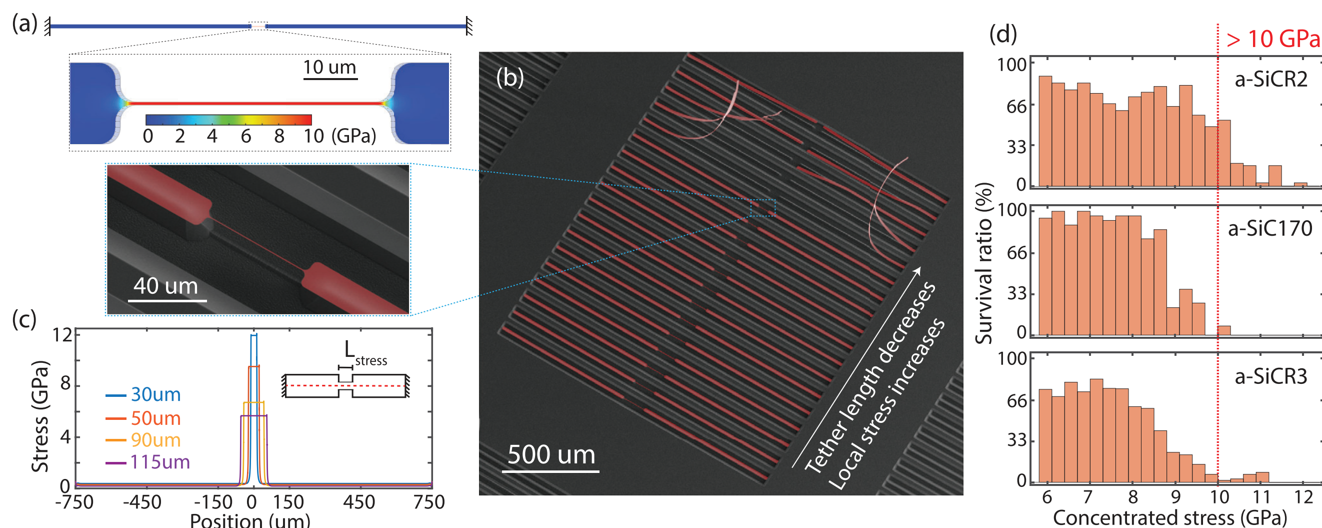

Figure 3. Tensile test experiment to measure the ultimate tensile strength of a-SiC thin films. a) Simulated stress profile of a hourglass-shaped geometry of 50 µm tether length made with a-SiCR2, the tensile stress is concentrated at the middle narrow tether up to 10 GPa, different maximum stress can be obtained with different tether lengths. b) SEM image of a pad of a-SiCR2 hourglass-shaped structures with 18 different tether lengths, from 30 to 115 µm. Below a certain tether length, the maximum stress surpass the ultimate tensile strength of the material, and the tethers break in the middle region after under-cutting, indicating the ultimate tensile strength of a-SiC. A zoom-in view of the hourglass-shaped geometry with a 50 µm tether length is shown on the left. c) The stress profiles along the hourglass-shaped geometries with different tether lengths. d) Survival ratios of hourglass-shaped geometries with maximum stress correspond to different stress interval (orange columns) for a-SiCR2 (top), a-SiC170 (middle), and a-SiCR3 (bottom). The maximum stresses shown for unbroken devices fabricated with a-SiCR2/a-SiC170/a-SiCR3 are 12.04/10.27/11.12 GPa, respectively.

during stress relaxation after suspending. As shown with FEM simulation in Figure 3c, devices with shorter tether lengths contain higher maximum concentrated tensile stresses on the tethers. This method allows the determination of the UTS of the nanostructured a-SiC thin films by counting the number of surviving devices after suspension. As shown in Figure 3b, a series of hourglass-shaped devices are fabricated with a-SiCR2. The 18 devices have tether lengths ranging from 30 to 115 µm, corresponding to stresses from 12.53 to 5.97 GPa, respectively. The adjacent devices have tether lengths that differ for 5 µm, the shorter the tethers are, the larger difference in concentrated stress the devices contain, for example the concentrated stress difference between devices with 115 and 110 µm tether lengths is 0.18 GPa, while one between devices with 35 and 30 µm is 0.72 GPa. In the case of each a-SiC thin film, the survival rate of each tensile interval shown in Figure 3d is determined, by employing 36 to 72 devices for testing.

The survival of the suspending hour-glass-shaped device with the tether length below 50 µm, corresponds to a UTS above 10 GPa for a-SiCR2. Similarly, we can identify the UTS for all a-SiC thin films used in this study to be >10 GPa, as shown in the histograms of ratios of survival devices in Figure 3d. The histograms also show that, with relatively higher deposition pressure and lower gas flow ratios, a maximum UTS up to 12 GPa can be achieved with a-SiCR2, which is almost twice that of the UTS shown for nanostructured LPCVD a-Si_3N_4 films. The measured UTS of a-SiCR4 is below 3.5 GPa, which is not attractive for further characterization. In the future, with a larger number of fabricated devices and a denser range of tether lengths, one can determine the UTS of the LPCVD a-SiC thin films more precisely. In practice, the nanopatterning with electron beam lithography can readily achieve an accuracy of 10 nm, which allows for the method's accuracy to be as low as 1.2 MPa on a-SiCR2, that is, an error of <0.2% when measuring the UTS. Higher UTS is found for recipes deposited with lower gas flow ratios (a-SiCR2/3/4), which might due to a higher carbon composition in the thin film,[44] and C-C chemical bonds are stronger than Si-C and Si-Si bonds.[63] For a-SiC films deposited with different pressure, a-SiCR2 (600 mTorr) is found to have a higher UTS, while a-SiC170 (170 mTorr) exhibits better yield under lower concentrated stresses as shown by the survival rates. According to the relationship between strength and Young's modulus E of SiC shown in ref. [49], UTS (or fracture strength) is 5.3% of E, therefore the theoretically predicted UTS for a-SiCR2/a-SiC170/a-SiCR3, are 11.82/11.66/11.13 GPa, respectively, matching well with the experimentally extracted data from the survived devices 12.04/10.27/11.12 GPa shown in Table 1. The small offset for the values of a-SiC170 may be due to its rougher surface as shown in Section S(G) (Supporting Information).

With strain engineering techniques, one can amplify the mechanical quality factor $Q = D_Q Q_0$ of a nanomechanical resonator by boosting their dissipation dilution factor D_Q, where Q_0 is the intrinsic quality factor of the thin film material.[10,64] Since the upper bound for D_Q of a nanomechanical string vibrating at a certain frequency ω is given by $D_Q \leq 12E\epsilon_{\mathrm{UTS}}^2/(\rho t^2\omega^2)$, where ϵ_{UTS} denotes the UTS of the thin film material,[65] thin-film materials with higher UTS and lower thickness are advantageous to obtain a higher D_Q. Among all a-SiC thin films shown in this work, a-SiCR2 is the most promising one to maximize the Q factor, thanks to its high Q_0 and UTS. The superior chemical resistivity of a-SiC enables the fabrication of thin films into suspending resonators with a thickness as low as 5 nm (shown in Section S(F), Supporting Information). This combined with its elevated ultimate tensile strength ϵ_{UTS}, which measures above

 © 2023 The Authors. Advanced Materials published by Wiley-VCH GmbH

15214095, 0, Downloaded from https://onlinelibrary.wiley.com/doi/10.1002/adma.202306513 by Technical University Delft, Wiley Online Library on [12/12/2023]. See the Terms and Conditions (https://onlinelibrary.wiley.com/terms-and-conditions) on Wiley Online Library for rules of use; OA articles are governed by the applicable Creative Commons License

15214095, 0, Downloaded from https://onlinelibrary.wiley.com/doi/10.1002/adma.202306513 by Technical University Delft, Wiley Online Library on [12/12/2023]. See the Terms and Conditions (https://onlinelibrary.wiley.com/terms-and-conditions) on Wiley Online Library for rules of use; OA articles are governed by the applicable Creative Commons License

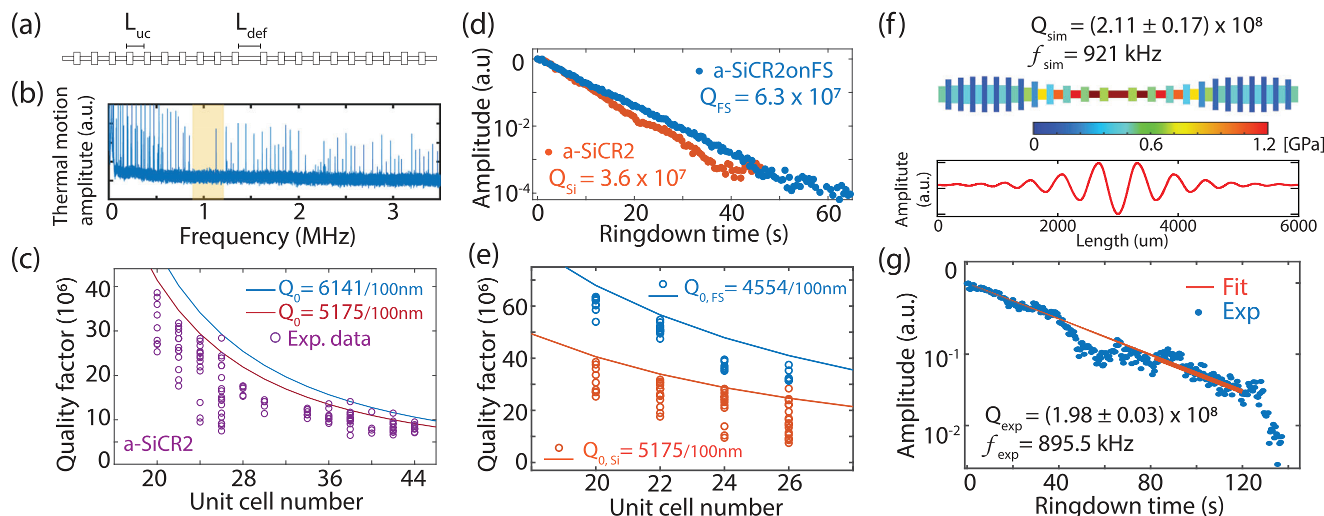

Figure 4. Intrinsic quality factor characterization and high Q factor a-SiC nanomechanical resonators optimized using Bayesian optimization. a) The geometry of the defect mode, of a 20 unit-cell (UC) PnC nanostring with unit cell length L_{uc} and defect length L_{def}. b) The measured frequency spectrum of a 20 UC PnC nanostring made with a-SiCR2. The yellow shaded area represents the engineered phononic bandgap. c) The intrinsic quality factor Q_0 of a-SiCR2 is measured with 20 to 44 UC PnC nanostrings. d) Ringdown measurements of 20 UC PnC nanostring made with a-SiCR2 (orange) and with a-SiCR2FS (blue). e) Comparison of the intrinsic quality factors Q_0 of a-SiCR2 (orange) and a-SiCR2FS (blue) with PnC nanostrings of 20 to 26 UC. The hollow rings and the solid line represent the measured Q factors and the numerical fittings respectively. f) The stress distribution (top) and mode shape of the defect mode (bottom) of the 6 mm tapered a-SiCR2 PnC nanostring optimized by Bayesian optimization. The optimized tapered PnC nanostring has 24 unit cells and a maximum stress of 1.2 GPa concentrated on the middle. g) Ringdown measurement of the optimized tapered PnC nanostring, high Q factor up to $Q_{exp} = 1.98 \times 10^8$ is measured.

10 GPa in thicker films, makes a-SiC string resonators highly promising in achieving a supreme upper bound for D_Q at a certain frequency ω.

5. Intrinsic Quality Factor and High Q Mechanical Resonators

In this section we characterize the intrinsic quality factor Q_0 of LPCVD a-SiC, then design and fabricate high-Q nanomechanical resonators with it. High mechanical quality (Q) factor nanomechanical resonators are desirable for various applications, ranging from precise force/acceleration sensing,[1,6] microwave-to-optical conversion,[66] to quantum optomechanics.[67,68] Following the method introduced by LIGO,[69] the field of strain engineering is advancing rapidly, boosting the Q factor of nanomechanical resonators by several orders of magnitude. A variety of strategies have been proposed aiming to improve the Q factors of tensile-loaded nanomechanical resonators. These include patterning 2D geometries appropriately,[9,11–13,70,71] modifying mass distribution[2,72] and mode of interest (e.g., from fundamental to higher order or from flexural to torsional modes[2]), in situ annealing for surface cleaning,[73] as well as cooling down to cryogenic temperatures.[14,74] The methods mentioned above can benefit from utilizing the LPCVD a-SiC thin film we characterized in this work, due to its high deposition film tensile stress, superior chemical resistivity, and impressive ultimate tensile strength.

The intrinsic quality factors Q_0 of a-SiC thin films are identified by experimentally measuring the Q factors of phononic crystal (PnC) nanostrings,[10] whose many spurious loss mechanisms are eliminated, and dissipation dilution factor D_Q is well defined, leading to an expected intrinsic Q factor $Q_0 = Q/D_Q$. For thin nanomechanical resonators, Q_0 can be assumed to depend linearly on the film thickness, since it is predominantly determined by surface loss rather than bulk loss.[64] We fabricate a series of uniformly corrugated high-aspect-ratio (PnC) nanostrings with a length of 4 mm, varying unit-cell lengths L_{uc} and defect lengths L_{defd} in the middle (**Figure 4**a), leading to PnC nanostrings with unit-cell numbers from 20 to 44. The widths of the wide and narrow parts of the nanostrings are 3 and 1 µm respectively. The vibration amplitude of the nanostrings as a function of frequency is acquired (Figure 4b) with a custom balanced homodyne detection interferometer at the vacuum environment of 4×10^{-9} mbar (see the schematic in the Experimental Section). Using the ringdown method, the Q factors of defect modes for each PnC nanostring are measured. For example, the ones of 10 unit-cells PnC nanostrings fabricated wtih a-SiCR2 and a-SiCR2FS are plotted in Figure 4d. Using FEM simulation, the dilution factor D_Q of each PnC nanostring geometry can be numerically calculated. Together with the Q factors of the corresponding nanostring measured experimentally, the intrinsic Q factor Q_0 of the different a-SiC thin films are determined. For example, the Q_0 of a-SiCR2 and a-SiCR2FS are shown in Figure 4c, e, respectively. The Q_0 of the other a-SiC films are shown in Table 1, and the corresponding measurement data can be found in Section S(D) (Supporting Information). In order to compare the Q_0 of a-SiC thin films with different thicknesses, we present them with the unit Q_0 per 100 nm, as Q_0 of a thin film is shown to be a function of thickness.[56] Deposited with the same recipe, a-SiCR2 (5175/100 nm) and a-SiCR2FS (4554/100 nm) have similar Q_0. The similar performance on the transparent substrate allows for integrating high-Q nanomechanical sensors into free-space optical systems in a practical manner. By reasonably assuming the

 © 2023 The Authors. Advanced Materials published by Wiley-VCH GmbH

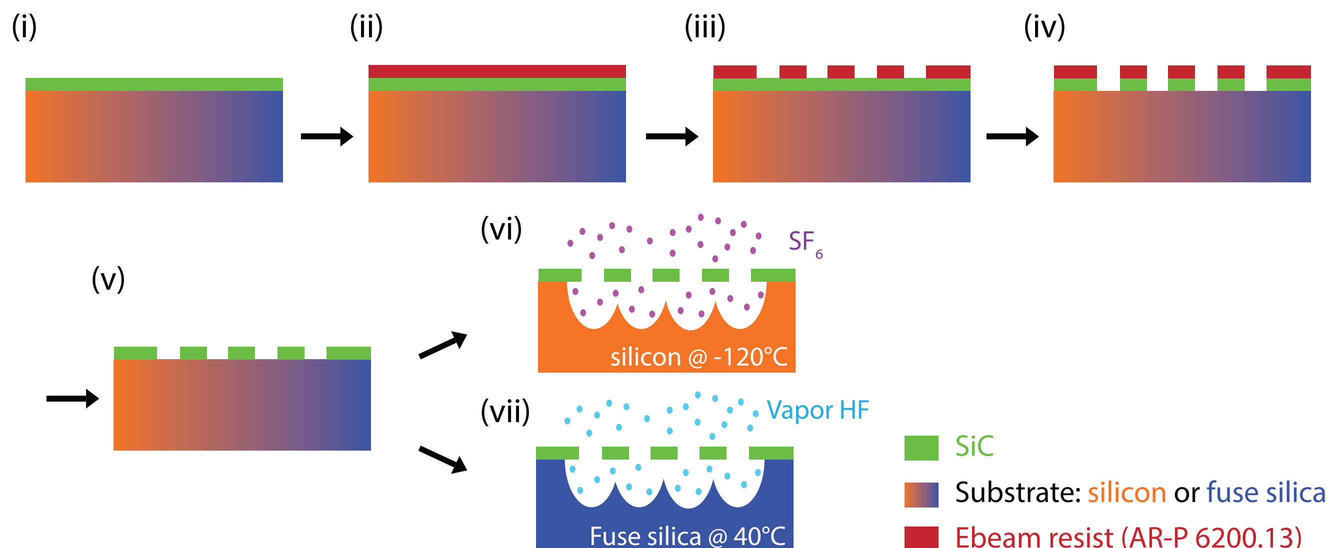

Figure 5. Fabrication process flow to fabricate a-SiC (green) nanomechanical resonators on both silicon (orange) and fused silica substrates (blue). i) Start with a die of the wafer. ii) Spin coat e-beam resist AR-P 6200.13 at spin speed 1500 rpm, then bake at 150 °C for 3 min. iii) E-beam pattern of the desired pattern, afterward developing the pattern by sequently immersing the die in pentyl acetate, MiBK:IPA = 1:1, IPA solutions for 1 min. iv) Transfer the pattern into the a-SiC film with reactive ion etching (Sentech Etchlab 200), with CHF_3/Ar plasma at a power of 60 W. v) Remove the e-beam resist with hot dimethylformamide solution in a supersonic bath, following by Piranha and diluted hydrofluoric acid cleaning. vi) Undercut the silicon substrate to suspend a-SiC resonators with cryogenic (−120 °C) SF_6 plasma etching. vii) Undercut the fused silica substrate to suspend a-SiC resonators with vapor hydrofluoric acid (at 35 to 60 °C).

films have similar mechanical properties on different substrates, a-SiCR2FS is measured to have a deposition stress of 1596 MPa, a factor of two higher than a-SiCR2 due to a larger thermal expansion coefficients difference between the a-SiC thin film and fused silica substrate. Worth noting is that the Q_0 of a-SiCR2 is the highest among all LPCVD a-SiC investigated, indicating that a lower and a moderate deposition pressure (600 mTorr) is beneficial to have better film quality.

To exploit the sensing potential of LPCVD a-SiC, we designed and optimized a tapered PnC nanostring with a length of 6mm and a thickness of 71 nm using a a-SiCR2 thin film. Bayesian optimization[12] was used to find designs with high Q-factor—more details can be found in Section S(E) (Supporting Information). This simulation-based optimization is largely possible due to the accurate characterization of the material properties of the a-SiC thin films in previous sections. As shown in Figure 4f, the optimized PnC nanostring consists of fixed 24 unit cells with different widths and lengths, leading to a stress concentration of up to 1.2 GPa toward its center part. Within the phononic bandgap generated by the optimized tapered PnC nanostring, a soft clamped defect mode with a simulated Q factor, $Q_{sim} = 2.11 \pm 0.17 \times 10^8$ appears at the frequency of $f_{sim} = 921$ kHz, as shown at the bottom of Figure 4f. The optimized tapered PnC nanostring was fabricated based on the design at the top of Figure 4f, and it was measured at an interferometer under ultrahigh vacuum of 4×10^{-9} mbar. As a result, an high Q factor mechanical mode with $Q = (1.98 \pm 0.03) \times 10^8$ was measured experimentally at a frequency of $f = 896$ kHz at room temperature, shown by its ringdown curve plotted in Figure 4g. This result demonstrates, for the first time, a mechanical quality factor exceeding 10^8 for silicon carbide nanomechanical resonators, as predicted by simulation. This also suggests that future design strategies to enhance resonator performance can be carried out using the LPCVD a-SiC thin films.

In addition, the quality factor-frequency product of the optimized LPCVD a-SiC tapered PnC nanostring is $Q \times f = 1.791 \times 10^{14}$, which is significantly higher than the quantum limit $Q \times f = 2\pi k_B T/\hbar = 6.24 \times 10^{12}$. This paves the way toward engineering quantum states in room temperature environments.[9,68] This high quality factor of the nanomechanical resonator with an effective mass $m_{eff} = 1.27 \times 10^{-13}$ kg corresponds to a force sensitivity of $\sqrt{S_F} = \sqrt{4k_B T m_{eff} \cdot 2\pi f/Q} = 7.7$ aN Hz$^{-1/2}$ at room temperature, which is comparable to a typical atomic force microscope cantilever operating at liquid helium temperature. With the high quality factor shown above, LPCVD a-SiC is shown to be the third material that can reach $Q > 10^8$ at room temperature using strain engineering, after conventional a-Si_3N_4[10] and strained silicon.[14] Moreover, the superior chemical and mechanical properties of LPCVD a-SiC allow for the fabrication of thinner and stronger resonators, enabling it to be more compatible with the dissipation dilution method. With advantages such as a relatively simple and low-cost fabrication process, compatibility with various substrates, including transparent ones, its high-Q performance, LPCVD a-SiC is a promising material for fabricating commercial mechanical sensors.

6. Conclusion and Outlook

Our study has uncovered an amorphous silicon carbide thin film with a ultimate tensile strength above 10 GPa, the highest value ever measured for a nanostructured amorphous material and approaching the experimental values shown by graphene nanoribbons.[24] Their robustness to chemicals allow us to

© 2023 The Authors. Advanced Materials published by Wiley-VCH GmbH

15214095, 0, Downloaded from https://onlinelibrary.wiley.com/doi/10.1002/adma.202306513 by Technical University Delft, Wiley Online Library on [12/12/2023]. See the Terms and Conditions (https://onlinelibrary.wiley.com/terms-and-conditions) on Wiley Online Library for rules of use; OA articles are governed by the applicable Creative Commons License

15214095, 0, Downloaded from https://onlinelibrary.wiley.com/doi/10.1002/adma.202306513 by Technical University Delft, Wiley Online Library on [12/12/2023]. See the Terms and Conditions (https://onlinelibrary.wiley.com/terms-and-conditions) on Wiley Online Library for rules of use; OA articles are governed by the applicable Creative Commons License

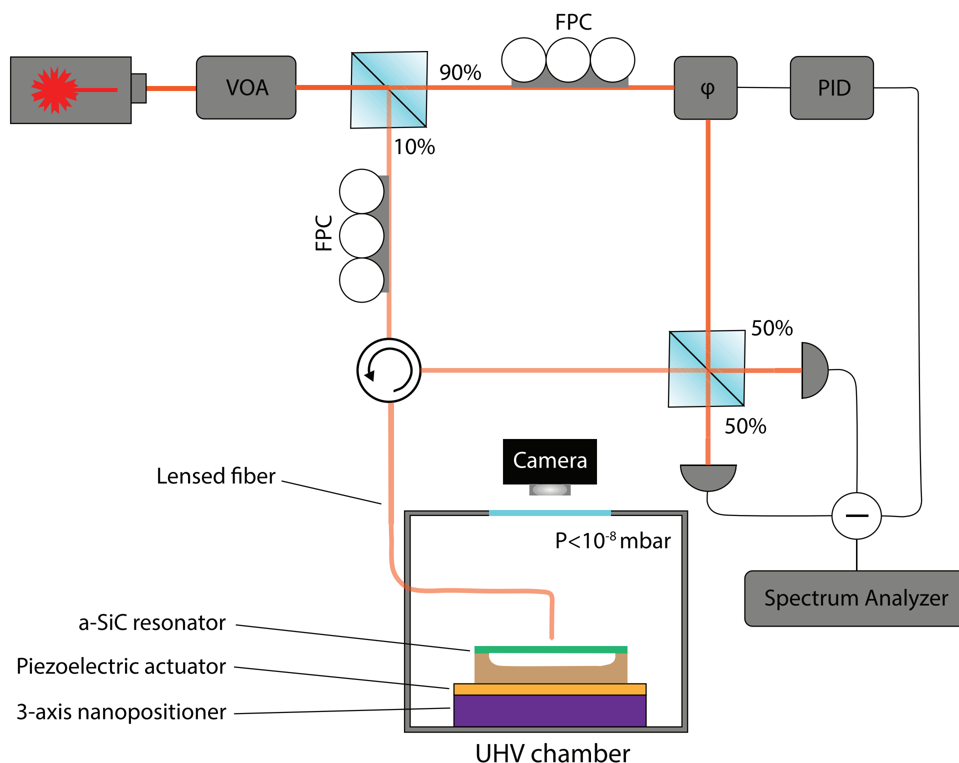

Figure 6. Schematic of the balanced homodyne interferometer used for performing ringdown experiments. The nanomechanical resonator, placed in an UHV chamber, is resonantly driven by a piezoelectric actuator, and its motion is measured with the interferometer. Abbreviations: VOA: variable optical attenuator; FPC: fiber polarization controller; φ: phase shifter; PID: proportional-integral-derivative controller.

fabricate nanostructures with very high fidelity even when their geometries make them delicate high-aspect-ratio structures. This ability to reliably produce structures also allow us to measure the film's mechanical properties with high precision. We deposit amorphous silicon carbide in varying deposition conditions and substrates to understand new approaches toward increasing ultimate yield strength. Then using the a-SiC with the highest UTS, we designed and fabricated a variety of well-understood nanostructures such as cantilevers, membranes and doubly clamped strings to measure the thin films mechanical properties such as density, Young's modulus, Poisson ratio, and mechanical loss tangent. For the latter we employ nanostrings patterned with phononic bandstructures which conventionally show some of the lowest mechanical dissipations in literature, and this allows us to measure very low mechanical dissipation. The a-SiC nanostrings support soft-clamped mechanical modes with quality factors exceeding 10^8 at room temperature; a new regime for SiC devices and on par with the state-of-the-art SiN resonators. This corresponds to a high force sensitivity of $\sqrt{S_\mathrm{F}} = 7.7$ aN Hz$^{-1/2}$. We demonstrate a robust characterization process based on the simple fabrication and optical techniques which does not rely on complex tension loading setups.

From molecular analysis of chemical composition (shown in Section S(H), Supporting Information), it appears that the elevated tensile strength in our a-SiC films is likely attributed to a higher prevalence of robust C–C bonds compared to weaker Si–Si bonds. This insight not only sheds light on the intricate interplay of bond structures and deposition parameters in determining mechanical resilience but also lays an understanding for further exploration in harnessing the unique properties of amorphous materials.

The discovery of this amorphous SiC material represents an advancement in the field of high-strength material science that is conventionally dominated by crystalline and 2D materials. However, our findings demonstrate that amorphous materials have the potential to surpass crystalline materials in certain applications due to their inherently isotropic mechanical properties, which allow for more design freedom and ease of fabrication. The high ultimate tensile strength of this amorphous material is particularly attractive for mechanical sensors, as it enables greater flexibility in strain engineering. This discovery opens up new possibilities for the use of amorphous materials in a variety of high-performance applications.

7. Experimental Section

7.1. Fabrication Process

Low pressure chemical vapor deposition (LPCVD) non-stoichiometric a-SiC films were used in this paper, deposited with different gas flow ratios (GFR) between SiH_2Cl_2 and 5% C_2H_2 in H_2 (GFR = 2, 3, 4), at various deposition pressures (170/600 mTorr), and on both silicon and fused silica substrates (Table 1). The variation in deposition parameters allowed to systematically characterize the mechanical properties of LPCVD a-SiC. All a-SiC films were deposited at a temperature 760 °C for

 © 2023 The Authors. Advanced Materials published by Wiley-VCH GmbH

the same period of time (3 h 20 min) to avoid film property differences caused by thermal effects and to ensure that the SiC films were composited of amorphous form instead of polycrystalline form.[44,75]

After LPCVD a-SiC deposition, the wafers were diced into smaller chips. The chips were then exposed to electron beam lithography to create desired patterns on the e-beam resist coated on top. Subsequently, these patterns were transferred into the a-SiC films using CHF_3 anisotropic plasma etching. Next, the patterned chips were cleaned with dimethylformamide and Piranha solution, followed by the undercut of the silicon substrate or fused silica substrate using cryogenic SF_6 isotropic plasma etching or vapor hydrofluoric acid. Finally, the designed a-SiC nanomechanical resonators were fabricated.

7.2. Ringdown Measurement with Homodyne Detection

A balanced homodyne interferometer was used for performing ringdown experiments on a-SiC nanoemchanical resonators. As shown in **Figure 5** and **Figure 6**, the a-SiC nanomechanical resonator (green) on top on the substrate (brown) was placed in an ultrahigh vacuum (UHV) chamber under a pressure $<10^{-8}$ mbar. This avoided mechanical losses due to gas damping. Ringdown measurements were performed via a piezoelectric actuator that resonantly drived the corrugated nanostrings. After reaching maximal amplitude, the drive was stopped to observe the rate at which mechanical energy was dissipated from the nanostrings. The vibration amplitude of the resonator was measured optically with a fiber coupled infrared laser (1550 nm). The power of the laser was divided into two parts, 90% of it was used for interference reference (local oscillator), while the other 10% terminated with a lensed fiber shines on the resonator. The reflected light from the resonator then compared its phase to the one from the local oscillator using the balanced homodyne measurement setup, with which the amplitude of the resonator was measured.

Supporting Information

Supporting Information is available from the Wiley Online Library or from the author.

Acknowledgements

The authors wish to acknowledge Peter G. Steeneken, Gerard Verbiest, and Martin Lee for their helpful suggestions on the manuscript and their support of our project. The authors also want to thank Satadal Dutta, Ali Sarafraz, Matthijs de Jong, Hanqing Liu for the helpful discussions. M.X. and R.N. also thank the staffs of both the Kavli Nanolab Delft and the Else Kooi Lab, in particular from Charles de Boer, for supporting the fabrication efforts, and from Hozanna Miro, for helping to perform the XRD measurement. The authors appreciate the help from P.R. Anusuyadevi and P. Gonugunta on the XPS measurement. This publication was part of the project, Probing the Physics of Exotic Superconductors with Microchip Casimir Experiments (740.018.020) of the research programme NWO Start-up which was partly financed by the Dutch Research Council (NWO). This work had received funding from the EMPIR programme co-financed by the Participating States and from the European Union's Horizon 2020 research and innovation programme (No. 17FUN05 PhotoQuant). R.N. would like to acknowledge support from the Limitless Space Institute's I^2 Grant. Funded/Co-funded by the European Union (ERC, EARS, 101042855). Views and opinions expressed are however those of the author(s) only and do not necessarily reflect those of the European Union or the European Research Council. Neither the European Union nor the granting authority can be held responsible for them.

Conflict of Interest

The authors declare no conflict of interest.

Data Availability Statement

The data that support the findings of this study are available from the corresponding author upon reasonable request.

Keywords

amorphous silicon carbide, high mechanical quality factor, ultimate tensile strength

Received: July 4, 2023
Revised: September 25, 2023
Published online:

[1] A. G. Krause, M. Winger, T. D. Blasius, Q. Lin, O. Painter, *Nat. Photonics* **2012**, *6*, 768.
[2] J. R. Pratt, A. R. Agrawal, C. A. Condos, C. M. Pluchar, S. Schlamminger, D. J. Wilson, *Phys. Rev. X* **2023**, *13*, 011018.
[3] T. Manzaneque, M. K. Ghatkesar, F. Alijani, M. Xu, R. A. Norte, P. G. Steeneken, *Phys. Rev. Appl.* **2023**, *19*, 054074.
[4] D. Garcia-Sanchez, K. Y. Fong, H. Bhaskaran, S. Lamoreaux, H. X. Tang, *Phys. Rev. Lett.* **2012**, *109*, 027202.
[5] J. M. Pate, M. Goryachev, R. Y. Chiao, J. E. Sharping, M. E. Tobar, *Nat. Phys.* **2020**, *16*, 1117.
[6] D. Hälg, T. Gisler, Y. Tsaturyan, L. Catalini, U. Grob, M.-D. Krass, M. Héritier, H. Mattiat, A.-K. Thamm, R. Schirhagl, E. C. Langman, A. Schliesser, C. L. Degen, A. Eichler, *Phys. Rev. Appl.* **2021**, *15*, L021001.
[7] C. Reinhardt, T. Müller, A. Bourassa, J. C. Sankey, *Phys. Rev. X* **2016**, *6*, 021001.
[8] S. S. Verbridge, J. M. Parpia, R. B. Reichenbach, L. M. Bellan, H. G. Craighead, *J. Appl. Phys.* **2006**, *99*, 124304.
[9] R. A. Norte, J. P. Moura, S. Gröblacher, *Phys. Rev. Lett.* **2016**, *116*, 147202.
[10] A. H. Ghadimi, S. A. Fedorov, N. J. Engelsen, M. J. Bereyhi, R. Schilling, D. J. Wilson, T. J. Kippenberg, *Science* **2018**, *360*, 764.
[11] S. A. Fedorov, A. Beccari, N. J. Engelsen, T. J. Kippenberg, *Phys. Rev. Lett.* **2020**, *124*, 025502.
[12] D. Shin, A. Cupertino, M. H. de Jong, P. G. Steeneken, M. A. Bessa, R. A. Norte, *Adv. Mater.* **2022**, *34*, 2106248.
[13] M. J. Bereyhi, A. Arabmoheghi, A. Beccari, S. A. Fedorov, G. Huang, T. J. Kippenberg, N. J. Engelsen, *Phys. Rev. X* **2022**, *12*, 021036.
[14] A. Beccari, D. A. Visani, S. A. Fedorov, M. J. Bereyhi, V. Boureau, N. J. Engelsen, T. J. Kippenberg, *Nat. Phys.* **2022**, *18*, 436.
[15] E. Romero, V. M. Valenzuela, A. R. Kermany, L. Sementilli, F. Iacopi, W. P. Bowen, *Phys. Rev. Appl.* **2020**, *13*, 044007.
[16] Y. S. Klaß, Ph.D. thesis, Technische Universität München, Munich, Germany **2022**.
[17] S. K. Manjeshwar, A. Ciers, F. Hellman, J. Bläsing, A. Strittmatter, W. Wieczorek, *Nano Lett.* **2023**, *23*, 5076.

© 2023 The Authors. Advanced Materials published by Wiley-VCH GmbH

15214095, 0, Downloaded from https://onlinelibrary.wiley.com/doi/10.1002/adma.202306513 by Technical University Delft, Wiley Online Library on [12/12/2023]. See the Terms and Conditions (https://onlinelibrary.wiley.com/terms-and-conditions) on Wiley Online Library for rules of use; OA articles are governed by the applicable Creative Commons License

[18] X. W. Gu, Z. Wu, Y.-W. Zhang, D. J. Srolovitz, J. R. Greer, *Nano Lett.* **2013**, *13*, 5703.
[19] X. Zhao, B. Mao, M. Liu, J. Cao, S. J. Haigh, D. G. Papageorgiou, Z. Li, R. J. Young, *Adv. Funct. Mater.* **2022**, *32*, 2202373.
[20] M. J. Bereyhi, A. Beccari, S. A. Fedorov, A. H. Ghadimi, R. Schilling, D. J. Wilson, N. J. Engelsen, T. J. Kippenberg, *Nano Lett.* **2019**, *19*, 2329.
[21] G. Kwon, H.-H. Jo, S. Lim, C. Shin, H.-H. Jin, J. Kwon, G.-M. Sun, *J. Mater. Sci.* **2015**, *50*, 8104.
[22] H. I. Rasool, C. Ophus, W. S. Klug, A. Zettl, J. K. Gimzewski, *Nat. Commun.* **2013**, *4*, 2811.
[23] T. Zhang, X. Li, H. Gao, *Int. J. Fract.* **2015**, *196*, 1.
[24] M. Goldsche, J. Sonntag, T. Khodkov, G. J. Verbiest, S. Reichardt, C. Neumann, T. Ouaj, N. von den Driesch, D. Buca, C. Stampfer, *Nano Lett.* **2018**, *18*, 1707.
[25] C. Lee, X. Wei, J. W. Kysar, J. Hone, *Science* **2008**, *321*, 385.
[26] M. Wang, C. Yan, L. Ma, N. Hu, M. Chen, *Comput. Mater. Sci.* **2012**, *54*, 236.
[27] J. Xu, G. Yuan, Q. Zhu, J. Wang, S. Tang, L. Gao, *ACS Nano* **2018**, *12*, 4529.
[28] R. Qu, M. Calin, J. Eckert, Z. Zhang, *Scr. Mater.* **2012**, *66*, 733.
[29] H. Jiang, T. Shang, H. Xian, B. Sun, Q. Zhang, Q. Yu, H. Bai, L. Gu, W. Wang, *Small Struct.* **2021**, *2*, 2000057.
[30] A. L. Greer, *Science* **1995**, *267*, 1947.
[31] M. Telford, *Mater. Today* **2004**, *7*, 36.
[32] M. Wijesundara, R. Azevedo, *Silicon Carbide Microsystems for Harsh Environments*, MEMS Reference Shelf, Vol. *22*, Springer Science & Business Media, Berlin, Germany **2011**.
[33] *Properties and Applications of Silicon Carbide*, (Ed.: R. Gerhardt), IntechOpen, London, UK **2011**.
[34] T. Kimoto, J. A. Cooper, *Fundamentals of Silicon Carbide Technology: Growth, Characterization, Devices and Applications*, Wiley-IEEE Press, Singapore **2014**.
[35] B. Morana, G. Pandraud, J. Creemer, P. Sarro, *Mater. Chem. Phys.* **2013**, *139*, 654.
[36] C. Iliescu, D. P. Poenar, in *Physics and Technology of Silicon Carbide Devices*, (Ed.: Y. Hijikata), IntechOpen, London, UK **2012**.
[37] T. Blum, B. Dresler, M. Hoffmann, St. Kaßner, *Surf. Coat. Technol.* **1999**, *116*, 1024.
[38] L. Jiang, X. Chen, X. Wang, L. Xu, F. Stubhan, K.-H. Merkel, *Thin Solid Films* **1999**, *352*, 97.
[39] S. Castelletto, A. Boretti, *J. Phys.: Photonics* **2020**, *2*, 022001.
[40] M. Köhler, M. Pomaska, P. Procel, R. Santbergen, A. Zamchiy, B. Macco, A. Lambertz, W. Duan, P. Cao, B. Klingebiel, S. Li, A. Eberst, M. Luysberg, K. Qiu, O. Isabella, F. Finger, T. Kirchartz, U. Rau, K. Ding, *Nat. Energy* **2021**, *6*, 529.
[41] L. Sementilli, E. Romero, W. P. Bowen, *Adv. Funct. Mater.* **2022**, *32*, 2105247.
[42] T.-K. Nguyen, H.-P. Phan, H. Kamble, R. Vadivelu, T. Dinh, A. Iacopi, G. Walker, L. Hold, N.-T. Nguyen, D. V. Dao, *ACS Appl. Mater. Interfaces* **2017**, *9*, 41641.
[43] H. A. Atwater, A. R. Davoyan, O. Ilic, D. Jariwala, M. C. Sherrott, C. M. Went, W. S. Whitney, J. Wong, *Nat. Mater.* **2018**, *17*, 861.
[44] B. Morana, Ph.D. thesis, TU Delft, Delft, The Netherlands **2015**.
[45] J. Chu, D. Zhang, *J. Micromech. Microeng.* **2009**, *19*, 095020.
[46] M. Imran, M. Mahendran, P. Keerthan, *J. Constr. Steel Res.* **2018**, *143*, 131.
[47] Y. Zhou, Y. Wang, P. Mallick, *Mater. Sci. Eng. A* **2004**, *381*, 355.
[48] K.-S. Chen, A. Ayon, S. M. Spearing, *J. Am. Ceram. Soc.* **2000**, *83*, 1476.
[49] J. Cui, Z. Zhang, H. Jiang, D. Liu, L. Zou, X. Guo, Y. Lu, I. P. Parkin, D. Guo, *ACS Nano* **2019**, *13*, 7483.
[50] D. J. Shuman, A. L. Costa, M. S. Andrade, *Mater. Charact.* **2007**, *58*, 380.
[51] J.-H. Kim, S.-C. Yeon, Y.-K. Jeon, J.-G. Kim, Y.-H. Kim, *Sens. Actuators, A* **2003**, *108*, 20.
[52] Y. S. Klaß, J. Doster, M. Bückle, R. Braive, E. M. Weig, *Appl. Phys. Lett.* **2022**, *121*, 083501.
[53] L. Barboni, G. Gillich, C. Chioncel, C. Hamat, I. Mituletu, in *IOP Conf. Series: Materials Science and Engineering*, Vol. *416*, IOP Publishing, Bristol, UK **2018**, pp. 012063.
[54] V. A. Chirikov, D. M. Dimitrov, Y. S. Boyadjiev, *Procedia Manuf.* **2020**, *46*, 87.
[55] S. Chen, *Ultrasonics* **2000**, *38*, 206.
[56] L. G. Villanueva, S. Schmid, *Phys. Rev. Lett.* **2014**, *113*, 227201.
[57] S. Wang, Z. Shan, H. Huang, *Adv. Sci.* **2017**, *4*, 1600332.
[58] A. Banerjee, D. Bernoulli, H. Zhang, M.-F. Yuen, J. Liu, J. Dong, F. Ding, J. Lu, M. Dao, W. Zhang, Y. Lu, S. Suresh, *Science* **2018**, *360*, 300.
[59] A. Shafikov, B. Schurink, R. W. van de Kruijs, J. Benschop, W. Van den Beld, Z. S. Houweling, F. Bijkerk, *Sens. Actuators, A* **2021**, *317*, 112456.
[60] M. D. Demetriou, M. E. Launey, G. Garrett, J. P. Schramm, D. C. Hofmann, W. L. Johnson, R. O. Ritchie, *Nat. Mater.* **2011**, *10*, 123.
[61] S. Zhang, Z. Li, K. Luo, J. He, Y. Gao, A. V. Soldatov, V. Benavides, K. Shi, A. Nie, B. Zhang, W. Hu, M. Ma, Y. Liu, B. Wen, G. Gao, B. Liu, Y. Zhang, Y. Shu, D. Yu, X.-F. Zhou, Z. Zhao, B. Xu, L. Su, G. Yang, O. P. Chernogorova, Y. Tian, *Natl. Sci. Rev.* **2022**, *9*, nwab140.
[62] T. Namazu, *IEEJ Trans. Electr. Electron. Eng.* **2023**, *18*, 308.
[63] J. Grunenberg, *Angew. Chem., Int. Ed.* **2001**, *40*, 4027.
[64] L. G. Villanueva, S. Schmid, *Phys. Rev. Lett.* **2014**, *113*, 227201.
[65] S. A. Fedorov, N. J. Engelsen, A. H. Ghadimi, M. J. Bereyhi, R. Schilling, D. J. Wilson, T. J. Kippenberg, *Phys. Rev. B* **2019**, *99*, 054107.
[66] T. Bagci, A. Simonsen, S. Schmid, L. G. Villanueva, E. Zeuthen, J. Appel, J. M. Taylor, A. Sørensen, K. Usami, A. Schliesser, E. S. Polzik, *Nature* **2014**, *507*, 81.
[67] J. D. Teufel, T. Donner, M. Castellanos-Beltran, J. W. Harlow, K. W. Lehnert, *Nat. Nanotechnol.* **2009**, *4*, 820.
[68] J. Guo, R. Norte, S. Gröblacher, *Phys. Rev. Lett.* **2019**, *123*, 223602.
[69] G. I. González, P. R. Saulson, *J. Acoust. Soc. Am.* **1994**, *96*, 207.
[70] Y. Tsaturyan, A. Barg, E. S. Polzik, A. Schliesser, *Nat. Nanotechnol.* **2017**, *12*, 776.
[71] Z. Li, M. Xu, R. A. Norte, A. M. Aragón, F. Van Keulen, F. Alijani, P. G. Steeneken, *Appl. Phys. Lett.* **2023**, *122*, 013501.
[72] D. Høj, F. Wang, W. Gao, U. B. Hoff, O. Sigmund, U. L. Andersen, *Nat. Commun.* **2021**, *12*, 5766.
[73] P. Sadeghi, Ph.D. thesis, Technische Universität, Wien, Vienna, Austria **2021**.
[74] T. Gisler, M. Helal, D. Sabonis, U. Grob, M. Héritier, C. L. Degen, A. H. Ghadimi, A. Eichler, *Phys. Rev. Lett.* **2022**, *129*, 104301.
[75] S. Nakao, T. Ando, L. Chen, M. Mehregany, K. Sato, in *2008 IEEE 21st Int. Conf. on Micro Electro Mechanical Systems*, IEEE, Piscataway, NJ, USA **2008** pp. 447–450.

© 2023 The Authors. Advanced Materials published by Wiley-VCH GmbH

15214095, 0, Downloaded from https://onlinelibrary.wiley.com/doi/10.1002/adma.202306513 by Technical University Delft, Wiley Online Library on [12/12/2023]. See the Terms and Conditions (https://onlinelibrary.wiley.com/terms-and-conditions) on Wiley Online Library for rules of use; OA articles are governed by the applicable Creative Commons License